THE FLAME DESCRIBING FUNCTION (FDF) UNIFIED FRAMEWORK FOR COMBUSTION INSTABILITY ANALYSIS : PROGRESS AND LIMITATIONS

Frédéric Boudy*[1,2], Thierry Schuller[1,2], Daniel Durox[1,2] and Sébastien Candel[1,2]

[1] CNRS, UPR 288, laboratoire EM2C, Grande voie des vignes, 92290 Châtenay-Malabry, France
[2] École Centrale Paris, Grande voie des vignes, 92290 Châtenay-Malabry, France
* Corresponding author: frederic.boudy@ecp.fr

Flame transfer functions are now commonly used to predict stability maps of various types of systems. Such linear analyses provide a rough estimate of the system stability, but do not give access to many phenomena observed in practice, e.g. amplitudes and frequencies of limit cycles, instability triggering or hysteresis. To account for these observations one has to represent the nonlinear response of the flame. One possibility which has been explored more recently consists in using experimentally determined Flame Describing Functions (FDFs). The method was validated in a generic multipoint injection system composed of an adjustable resonant upstream manifold and different quartz tubes to confine the flame. In general, predictions are in good agreement with measurements when the limit cycle features an essentially constant amplitude. Nevertheless, it is found that in certain parameter ranges many of the limit cycles feature a time variable amplitude. The present article encompasses all the limit cycles, with constant or time variable amplitude, characterized on the multiple flame combustor. For time-varying amplitude, the describing function does not generally provide correct estimates and cannot be used to represent the unsteadiness in limit cycle level, but this methodology allows to identify conditions giving rise to such phenomena and it yields bounds on the amplitude levels and frequencies for some cases.

1 Introduction

The Flame Describing Function (FDF) framework has been devised to fill the gap between observations carried-out at limit cycles and predictions of thermoacoustic instabilities. The describing function method originates from nonlinear control theory (see for example [1]). In general approach is applicable when there is a single nonlinear element (in the present case, this component is the flame) and that the other units in the system filter out higher order harmonics so that the system stability is essentially governed by the fundamental frequency component. The describing function is constituted by a family of transfer functions measured or calculated for a set of amplitudes.

One objective of the FDF method has been to encompass the definition of instability regions, obtain instability characteristics and estimate limit cycle amplitudes and frequencies. Another objective is to interpret the many nonlinear features manifested in practical systems such as mode switching, nonlinear triggering, frequency shifting. The describing function methodology is dedicated to the modeling the combustion dynamics in burners where the flame response to flow perturbations is nonlinear, but the resulting acoustic perturbations within the system remain in the linear range. This corresponds to

situations where the higher order harmonics are filtered out by the combustor acoustics, so that the system stability is essentially governed by the fundamental frequency component.

The application of the describing function concept to nonlinear flame dynamics were attempted in some recent studies. One possible saturation mechanism giving rise to limit cycles is envisaged in [2] to represent the motion of a ducted flame stabilized on a bluff-body [3]. In this analysis based on the describing function (DF) methodology borrowed from control theory, the flame gain saturates when the flow at the bluff-body is reversed. A more advanced model of the flame motion [4] analyzed in the DF framework yields predictions of the unstable amplitude and frequency. The nonlinear transfer function concept is also used in [5] to analyze the dynamics of a combustor submitted to equivalence ratio fluctuations. The transfer function was calibrated by making use of experimental data and suitable estimates of limit cycles were obtained by considering the mean air-fuel ratio as a bifurcation parameter.

A unified framework combining a measured flame describing function with an acoustic network was developed to examine the stability of a burner with an unconfined flame [6] and reproduce the nonlinear features observed in the experiments. This was later extended to deal with generic burner with a confined flame [7, 8]. Systems including turbulent premixed swirled flames were also recently investigated using the same methodology [9, 10]. By taking into account the nonlinear dependence of the flame response with respect to the input level, it was possible to reproduce the limit cycles observed in experiments. In addition, this nonlinear treatment gives access in many cases to the nonlinear features observed in practice, e.g. hysteresis or triggering [6, 8]. In a recent theoretical analysis [11], the authors examined the nonlinear stability of a Rijke tube comprising a diffusion flame by using different techniques. The results indicate that the FDF methodology enabled to find the expected limit cycles. In many situations, the FDF is measured experimentally to obtain the correct flame frequency response when the perturbation amplitude is varied.

One interesting feature with the multipoint injection system investigated by [12] is the variety of nonlinear dynamical phenomena observed. The present study is aimed at testing the FDF methodology when the flame tube length is varied giving rise to many distinct situations. Experiments and calculations have already been reported in [7, 8] for short flames tubes. It was found that limit cycles, hysteresis, triggering and mode switching observed by changing the feeding manifold length were fairly well retrieved by calculations. The FDF framework was however less successful in predicting the unstable behavior observed with the longer confinement tube [7].

Even if an overall agreement was found between measurements and predictions for most of the geometries, further analysis revealed unusual cases where the limit cycle features a time-varying amplitude typified by more complex oscillations. For example, cyclic oscillations were found for a short flame tube in [13], while more chaotic oscillations were reported in [14]. In a recent investigation, [15] also describes observations of nonstandard types of oscillations in a multiple flame combustor equipped with a perforated plate comprising a small number of holes. The flame tube size is used as a bifurcation parameter providing access to a variety of limit cycles. Their investigation through nonlinear time series analysis allows to delineate the different dynamical phenomena. The objective of the present study is to explore the limitations of the FDF methodology by investigating the various types of limit cycles observed in the generic configuration considered by Boudy [12].

This article begins with a short description of the test rig and instrumentation. The FDF analysis is reported next with a brief presentation of typical results. Then, the different types of limit cycles observed in the setup are analyzed. FDF calculations are then used to delineate the subtending processes and sort out the different mechanisms contributing to the observed time-varying amplitudes.

2 Experimental setup and typical combustion regimes

The experimental setup is sketched in Fig. 1. The burner can be divided into three parts. A feeding manifold of radius R_1 = 0.035 m terminated by a perforated plate which delivers a premixed stream. The perforated plate anchors a collection of small laminar conical flames. The third element is an open ended quartz tube of radius R_2 = 0.065 m, enclosing the combustion zone. A piston is used to easily modify the length of the feeding manifold during experiments. This length L_1 measured between the upstream side of the perforated plate and the head of the piston was varied in discrete steps all the way

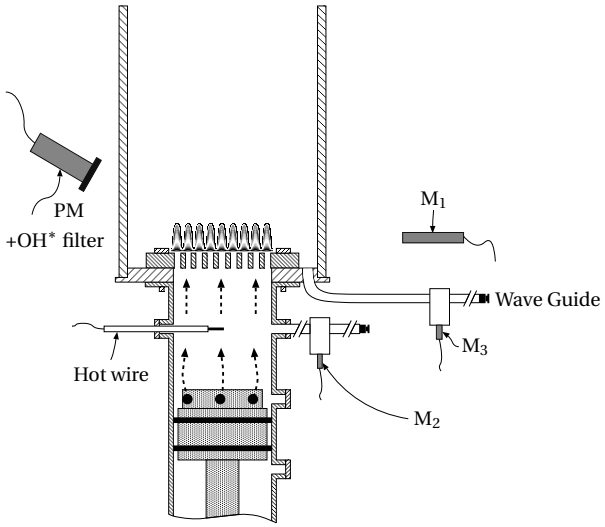

Figure 1: Experimental setup used to characterize self-sustained combustion oscillations and associated diagnostics. Three microphones are used to measure the pressure fluctuations. Microphone M_1 is located 0.25 m away from the burner axis while microphones M_2 and M_3 are connected to 25 m waveguides. A hot wire probe measures the velocity fluctuations in the feeding manifold. A photomultiplier equipped with an OH* filter gathers light radiated by the flame through the quartz tube and measures the OH* light intensity fluctuations.

from L_1 = 0.11 m to 0.55 m. By using an additional tube, it is possible to sweep the feeding manifold length from L_1 = 0.11 m to 0.77 m. The head of the piston is designed to offer a nearly perfect reflecting boundary for acoustic waves. It is machined with a small peripheral shoulder with six holes on the periphery to allow flow of the premixed reactants to be injected in the cavity. The flame tube of size L_2, can also be changed. Four quartz tubes of different lengths are used ranging from L_2 = 0.10 m to L_2 = 0.40 m by steps of 0.10 m. The perforated plate located at the top of the feeding manifold and confined within the quartz tube, anchors a collection of small laminar conical flames. It has a thickness l = 3 mm or l = 15 mm and a diameter $2R$ = 70 mm. It is made of stainless steel and comprises N = 421 holes of diameter $2r_p$ = 2 mm arranged on a 3 mm square mesh, resulting in a global porosity $\mathscr{P} = N\pi r_p^2/\pi R^2$ of 0.34. Experiments are carried out with a methane/air mixture of flow rate $\dot{m}$ = 4.7 g.s^{-1} at an equivalence ratio ϕ = 1.03, providing a thermal power of P = 13.3 kW for different geometrical configurations by modifying L_1 or L_2.

The setup is equipped with different probes allowing measurements of velocity, pressure and heat release rate fluctuations. Figure 1 shows the burner and associated diagnostics and sensors. Five quantities are measured in this experiment. Velocity fluctuations are determined by means of a hot wire probe 3 cm below the perforated plate. Three microphones are used to record pressure fluctuations at different locations on the burner. Microphone M_1 records the sound radiated at 0.25 m away from the burner axis. Pressure fluctuations inside the burner are measured by two microphones connected to waveguides terminated by a 25 m channel. These channels are sufficiently long to avoid wave reflection. Microphone M_2 is connected to the feeding manifold while M_3 is plugged on the waveguide connected to the flame plane. Different plugs are located along the feeding manifold length L_1. They are separated by 5 cm from each other and microphone M_2 is plugged on the first one facing a hot wire. A photomultiplier equipped with an OH* filter (λ=308 nm) records the radical emission from the flame, which is proportional to the heat release rate [16,17]. Measurements are processed with LabVIEW® and Matlab®.

The experimental investigation begins by setting a confinement tube L_2 with the head of the piston L_1 close to the perforated plate. Then, the system is ignited and the piston is moved from minimum to maximum extension with a predefined step. Once the maximum extension has been reached, another

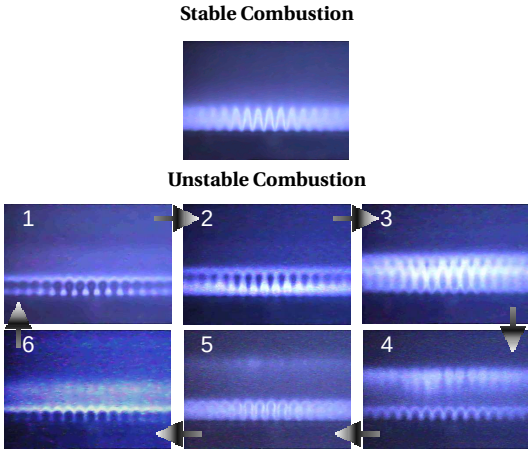

Figure 2: Stable (L_1 = 0.25 m) and unstable (L_1 = 0.29 m) combustion regimes. These records illustrate typical flame dynamics observed in the burner. L_2 = 0.10 m, thin perforated plate l = 3 mm.

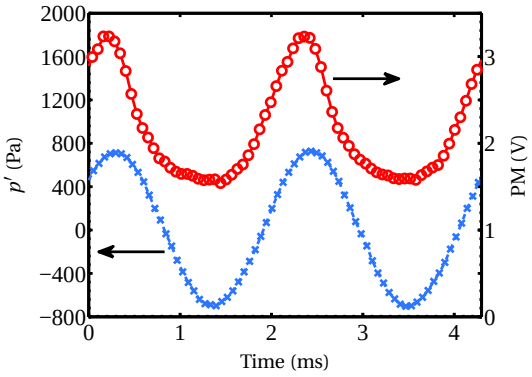

Figure 3: Pressure signal from microphone M_2 (left vertical axis) and OH* radicals light intensity (right vertical axis) under self-sustained oscillations. The burner is equipped with a thin perforated plate l = 3 mm. The feeding manifold is adjusted to L_1 = 0.51 m with a flame tube L_2 = 0.20 m.

sweep is undertaken in the reverse direction (maximum to minimum). Depending on the piston position L_1 and the confinement tube L_2 selected, combustion is either stable or unstable. In a stable case, flames have a steady conical shape with a low level of noise reaching about 100 dB at microphone M_2 (reference pressure 2×10^{-5} Pa). This is illustrated in Fig. 2. In this case, L_1 = 0.25 m, L_2 = 0.10 m and the burner is equipped with a thin perforated plate l = 3 mm.

In a typical unstable case, all the flames move in a synchronized fashion with formation and collapse of fresh reactant pockets as illustrated in Fig. 2. In this latter case, the feeding manifold length is set to L_1 = 0.29 m. This oscillation is typified by a well defined frequency f = 750 Hz and a constant amplitude with a high noise level in excess of 140 dB at microphone M_2. For longer flame tubes, higher oscillation levels may be reached during unstable operation and the flame motion is often more complex.

Typical pressure and heat release rate fluctuations recorded in the system are plotted in Fig. 3 for a different flame tube L_2. The pressure signal remains sinusoidal whereas the OH* radicals light intensity signal, corresponding to the heat release rate, shows asymmetrical oscillations, revealing the nonlinearity of the flame response. In these experiments, the pressure is essentially harmonic, indicating that the acoustic field remains in the linear range. Unstable regimes are therefore examined with the FDF framework in the next section.

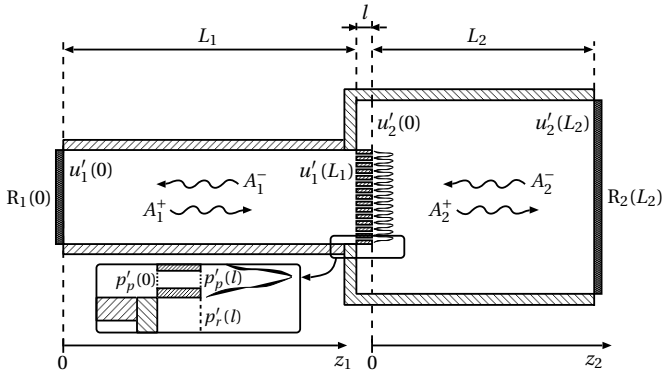

Figure 4: Burner and definitions used for in the thermo-acoustic analysis.

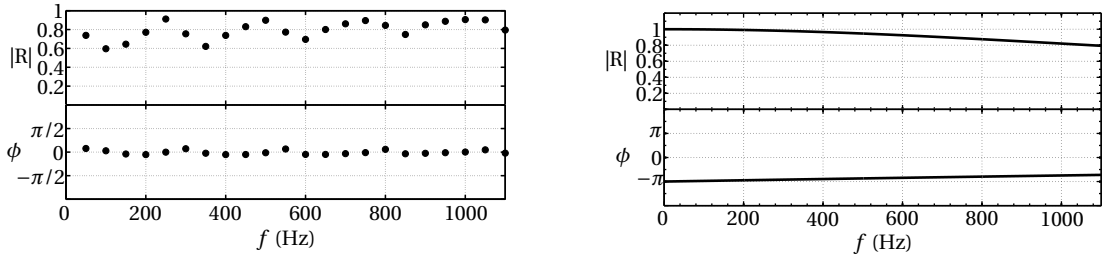

Figure 5: Left : Reflection coefficient of the piston head measured for a nominal flow rate of 4.7 g s^{-1}. Right : Reflection coefficient $R_2(L_2)$ of the confinement tube outlet. The temperature is fixed to $T_2 = 900$ K.

3 Nonlinear approach and FDF analysis

The combustor features low frequency unstable modes and one may thus consider that the wave motion is longitudinal and takes place in the axial direction z. The pressure oscillations detected remain relatively weak compared to the mean pressure ($p'/p \approx 1$ %) and the analysis is carried out by assuming that acoustic disturbances are linear. Moreover, the system operates at a low Mach flow number ($M \leq 0.01$) so that flow effects can be neglected in the analysis of acoustic propagation. The system is modeled by a set of compact acoustic elements represented schematically in Fig. 4. The model comprises two cylindrical cavities, a flame zone with a ring cavity between these two elements, and two boundary conditions at the system inlet and exhaust. The mean temperature $\overline{T_n}$ and density $\overline{\rho_n}$ are considered to be uniform in each cavity n. The piston head reflection coefficient $R_1(0)$ was determined experimentally (Fig. 5-left). The reflection coefficient of the outlet $R_2(L_2)$ is represented by taking into account sound radiation from an unflanged open pipe [18, 19] (Fig. 5-right). Dissipation in the perforated plate used as a flame holder is modeled with a relation due to Melling [20]. The contribution from the ring cavity surrounding the flame is also taken into account in the network [12].

The flame response to flow perturbations is included in the model by using the FDF determined experimentally in a separate set of experiments [7, 8]. This describing function is determined for forcing frequencies ranging from 0 to 1600 Hz and different perturbation amplitudes. This is accomplished by subjecting the flame sheet to harmonic fluctuations by means of a loudspeaker [21]. It should be noted that measurements of the FDF were carried out with and without flame tube to ensure that there was no significant change between these configurations. Measurements without flame tubes are easier as the confinement tube promotes self-sustained combustion oscillations, hindering any control from the loudspeaker both in frequency and amplitude. These measurements are not presented here for conciseness, but can be found in [12]. It was found that the flame response does not depend on the flame

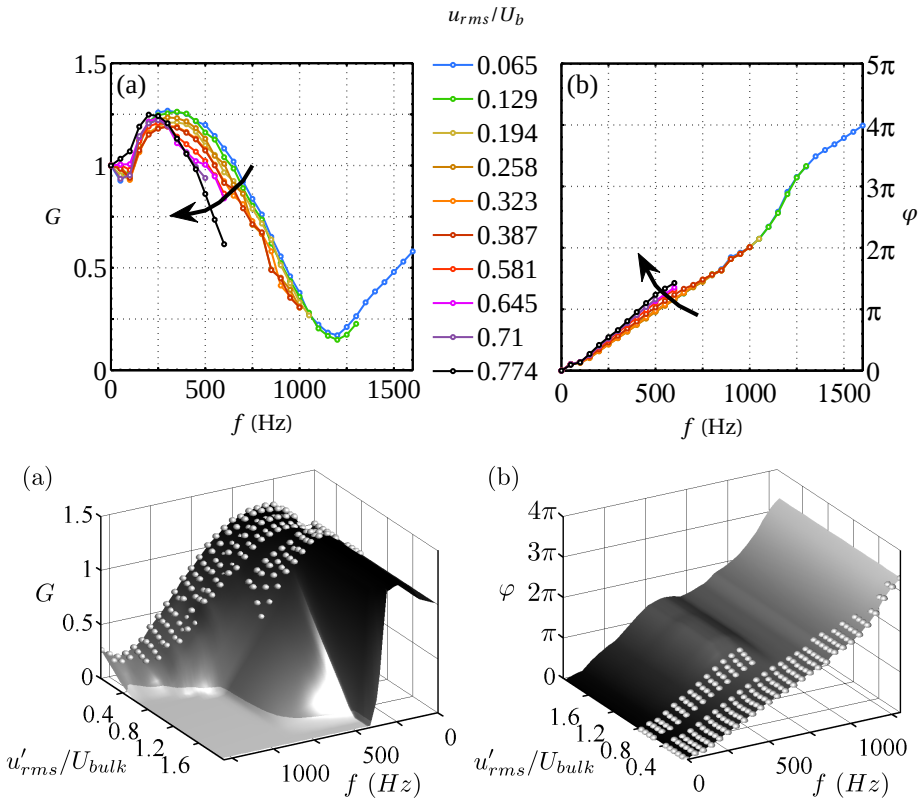

Figure 6: Top : FDF measurements as a function of the forcing frequency for different perturbation amplitudes, where u_{rms} corresponds to the rms value of the fluctuation amplitude and U_b the mean flow velocity within one perforation of the flame holder. The perforated plate thickness is set to l = 15 mm with a short flame tube L_2 = 0.10 m. A gray scale shows the increasing level of fluctuations. (a) FDF gain G, (b) FDF phase lag φ. Bottom : Interpolated and extrapolated FDF used in the calculations. Measurements are shown by small spherical symbols.

tube. It must be stressed that the configuration explored comprises a collection of small laminar conical flames embedded in a confinement tube having a larger diameter. One might not infer the same conclusions for other flame configurations. For example, the flame response studied in [22] is modified when the flame tube diameter is decreased, which leads to interactions between the flame and the cold wall. The flame response is also modified when the burnt gases cannot fully expand as demonstrated in a recent analysis [23]. FDF measurements were carried out over a frequency and amplitude ranges which are bounded by the loudspeaker efficiency at high amplitude and high frequency. In the missing areas, high amplitude self-sustained combustion oscillations were used for interpolation and extrapolation of the flame response. These data are presented in Fig. 6 for a plate of thickness l = 15 mm and a flame tube L_2 = 0.10 m. The gain G is drawn in Fig. 6(a) and the phase lag φ appears in Fig. 6(b).

When the amplitude increases, the gain G drops and phase lag φ is shifted to higher values, confirming the nonlinear flame behavior. The flame also acts as a low pass filter with a significant overshoot at higher frequencies and low fluctuation amplitudes. It is worth noting that the phase lag φ evolves in a quasi linear fashion with frequency and is sensitive to the fluctuation level.

4 Comparison between calculations and measurements

The elements described in the previous section are combined to compute the stability map of the burner for different geometries. Calculations and comparison with measurements at the limit cycle are

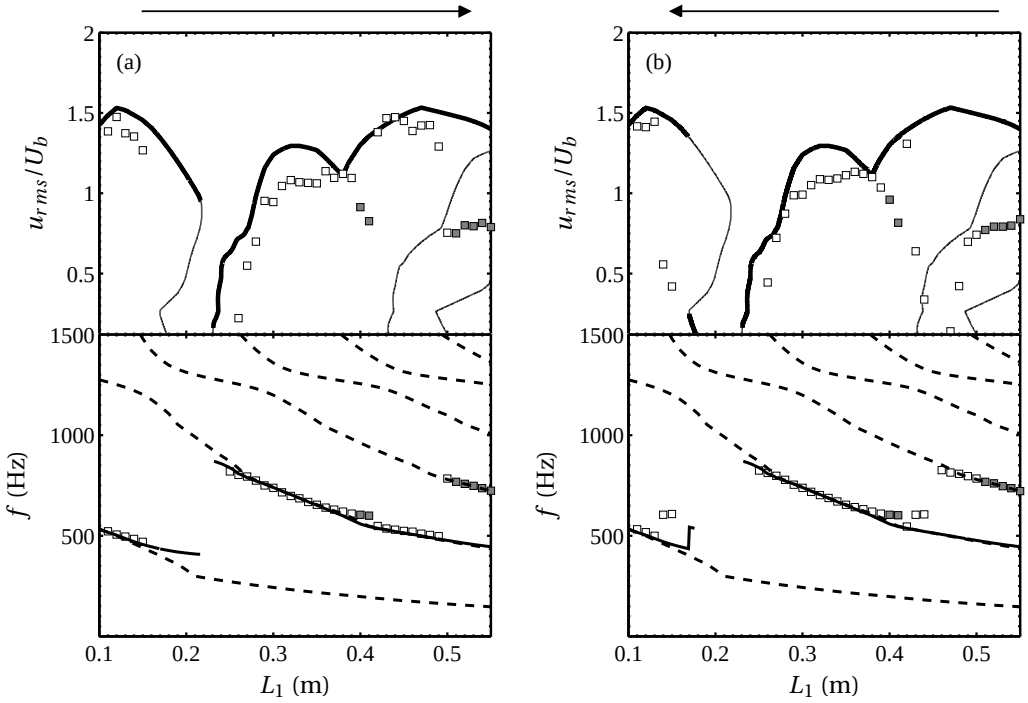

Figure 7: Comparison between measurements and predictions for the short flame tube $L_2 = 0.10$ m. The feeding manifold length L_1 is swept from $L_1 = 0.11$ m to 0.55 m (a) and in the reverse direction $L_1 = 0.55$ m to 0.11 m (b). The bold lines indicate limit cycle predictions. Amplitudes and frequencies observed in the experiment are indicated by m square symbols (□). Open symbols pertain to limit cycles with a stable oscillation level. The gray symbols reveal situations with unstable amplitude and frequency. In this latter case, the main frequency peak of the pressure spectrum is shown in the diagram. The dashed lines correspond to the acoustic eigenmodes calculated without unsteady combustion.

here illustrated for a single flame tube length $L_2 = 0.10$ m. The reader is referred to references [7, 12] for details on the nonlinear stability analysis and determination of the limit cycle amplitudes and frequencies when the feeding manifold length L_1 is swept between 0.11 m and 0.55 m in both ways. Limit cycle frequencies f and fluctuation levels u_{rms}/U_b found in calculations are compared to measurements in Fig. 7 as a function of the feeding manifold length L_1.

Results for the first exploration direction ($L_1 = 0.11$ m to 0.55 m) are drawn on the left, while the reverse direction results appear on the right hand side. Calculations of limit cycle amplitudes and frequencies show that predictions agree with measurements for many configurations. These calculations also capture the system hysteresis confirming what was found in previous studies [6, 8].

Measurements at limit cycles however indicate that for certain lengths of the feeding manifold L_1, the oscillation amplitude is not stabilized at a fixed level. In these cases the signal was processed band-pass filtered around the fundamental frequency of the pressure spectrum. Then, the amplitude and frequency of this signal were used for comparison with calculations leading to a lesser degree of agreement. The experimental level is generally lower than the predicted value. Calculations carried out for the other flame tubes under similar conditions are not presented here for conciseness, but they exhibit the same type of features.

To synthesize the main results, the FDF framework enables to predict the unstable regimes observed in the setup when the feeding manifold or the flame tube length are varied. One obtains suitable estimates of the oscillation amplitude occurring in the system. Nevertheless, the method is valid when

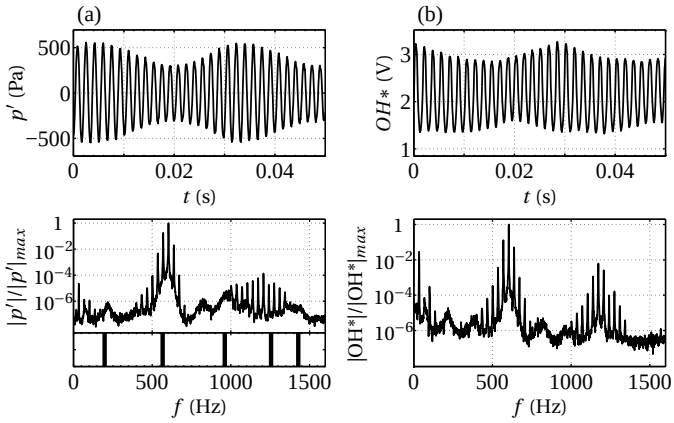

Figure 8: Pressure signal recorded by microphone M_2 and OH* light emission for L_1 = 0.40 m and L_2 = 0.10 m. Corresponding spectral densities are shown below the signals. The window under the pressure spectrum on the left shows the acoustic modal frequencies as vertical solid lines calculated without combustion.

the oscillation level and frequency of the limit cycle remain constant in time. In the broad experimental range of the present investigation, some geometries are typified by new kinds of limit cycles where amplitude and frequency evolve as a function of time. This variety is sometimes described in the literature [15]. In these cases, the spectral analysis shows multiple frequency peaks and the FDF model predictions do not necessarily with experimental data as shown in Fig. 7. These limit cycles are typified by perturbed sound signatures which differ from the more standard single frequency cases. It is then logical to examine these cases in a systematic fashion to sort out the various types of limit cycles with time-varying amplitudes. It is still useful to examine results of the FDF methodology to try to predict domains where such situations prevail.

5 Analysis of time-dependent limit cycles

5.1 Interaction with acoustic boundary

It has already been shown that nonlinear interactions taking place at the combustor extremities are able to change a limit cycle [24]. In the configuration explored herein, it is shown that destabilization of the limit cycle can also take place due to a purely linear interaction with one of the acoustic boundary condition. This type of phenomenon appears for the instabilities observed with the short flame tube L_2 = 0.10 m at two feeding manifold lengths L_1 = 0.40 m and 0.41 m. In these cases, the pressure spectral density show multiple peaks with high amplitudes. This is illustrated in Fig. 8 for the pressure and PM signals when L_1 = 0.40 m. These signals exhibit modulations because oscillation frequencies are close. The flame spectrum is typified by a series of concentrated peaks around the main instability frequency. One can easily distinguish three main components with a peak at 604 Hz, a lower peak at 570 Hz and a third component at 638 Hz. These three frequencies lie around the second acoustic mode of the system calculated without unsteady combustion. The pressure signal is further analyzed by using the continuous wavelet transform with a complex Morlet mother wavelet to characterize the frequency evolution with time. The resulting analysis presented in Fig. 9 indicates that the instability frequency oscillates around a mean value and that the oscillation frequency reaches a maximum when the pressure oscillation reaches a minimum and conversely.

Measurements are now compared to FDF calculations in Fig. 10, where the growth rate and frequency trajectories are plotted as a function of the perturbation amplitude u_{rms}/U_b. Calculations indicate that the second eigenmode of the system is unstable. Results reveal an overall agreement between calculations and experiments with a few differences. The oscillation state is well captured with for the max-

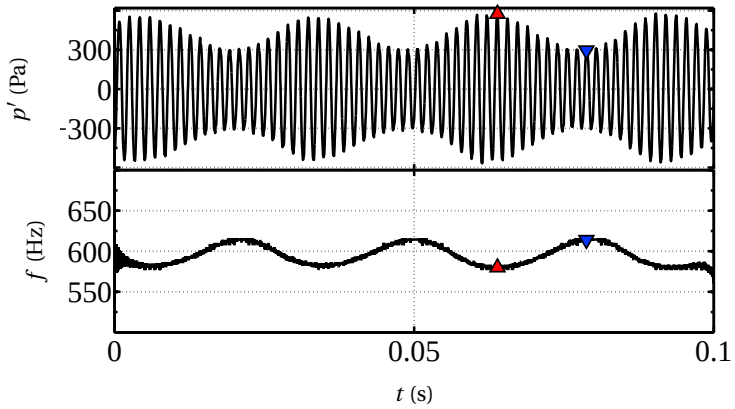

Figure 9: Top : Pressure signal from microphone M_2 for L_1 = 0.40 m and the short flame tube L_2 = 0.10 m. Bottom row : Evolution of frequency with time as the amplitude increases or decreases. Two symbols indicate the minimum and maximum amplitudes reached with their respective frequency.

imum amplitude indicated by the upward-pointing triangle symbol (red), but the minimum amplitude shows less agreement with the trajectories as indicated by the downward-pointing triangle symbol (blue).

It is now interesting to examine the origin of this regular modulation. To this purpose, the frequency range of this phenomenon is superimposed on the reflection coefficient of the piston head presented before and plotted in Fig. 11. It is striking to see that this frequency range corresponds to a situation where the reflection coefficient modulus features a "V" cusp between 580 Hz and 620 Hz. An almost equal modulus $|R_1(0)|$is found for these two frequencies without phase shift at 580 Hz and a small one at 620 Hz. This defines a band where small frequency variations are correlated to large changes in the reflection coefficient. One possible scenario is that at high amplitude, low frequency sound waves are damped to a lesser extent than at high frequency. The oscillation amplitude increases but the frequency also, as shown by the FDF calculations in Fig. 10 for high perturbation amplitudes. Between u_{rms}/U_b = 1 and 1.3, the slope of the frequency trajectory is positive. Thus, after an initial growth with a frequency decrease, it increases and the amplitude falls down. Then, growth rate becomes positive and the oscillation level grows again and so on. This sustains a modulation of the limit cycle both in amplitude and frequency. By examining the reflection coefficient, the same "V" cusps are identified for other frequency bands where the modulus features this singularity.

Analysis of this first type of time-dependent limit cycle reveals that the FDF framework can be used to determine the unstable state of the burner, even if the amplitude and frequency are not well stabilized. One is still able to deduce the general evolution of amplitude and frequency of oscillation from the FDF calculations by examining the frequency and growth rate trajectories as a function of the amplitude u_{rms}/U_b. It is also possible to show that modulation of the limit cycle amplitude and frequency result from interactions of acoustic waves with a singularity in the response of the acoustic boundary at the combustor inlet. In practical systems, it is not rare to have a complex acoustic response of elements upstream or downstream of the combustor, an original mechanism which may be at the origin of time modulations of limit cycle characteristics.

5.2 Interactions between multiple modes

Interactions between multiple modes are known to lead to combustion instabilities with multiple frequencies as explored theoretically by [25] or [26] where it is shown that this can happen if two modes exist of which one is stable and the other is unstable. This is illustrated here in a situation where a linearly unstable mode triggers a nonlinearly unstable mode at a different frequency. In many situations

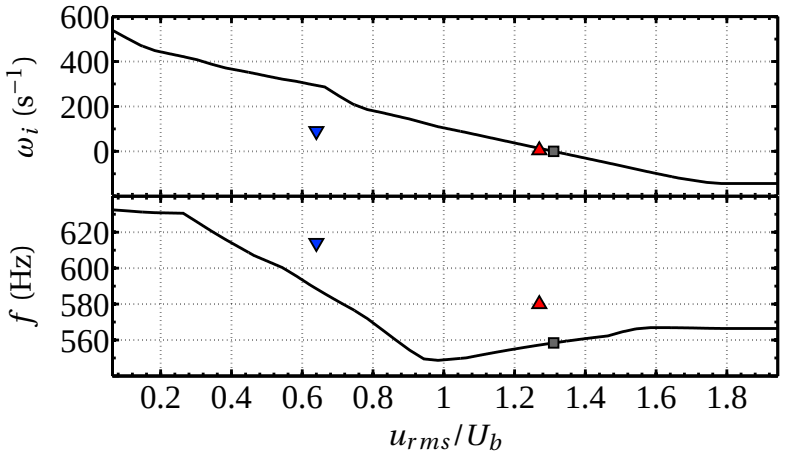

Figure 10: Growth rate ω_i and frequency f evolution as a function of the relative fluctuation amplitude u_{rms}/U_b. The limit cycle found by analyzing the growth rate trajectory is marked as a gray square symbol. Results from the time frequency analysis in Fig. 9 are indicated by the downward-pointing triangle symbol (blue) for the minimum oscillation amplitude and by the upward-pointing triangle symbol (red) for the maximum amplitude.

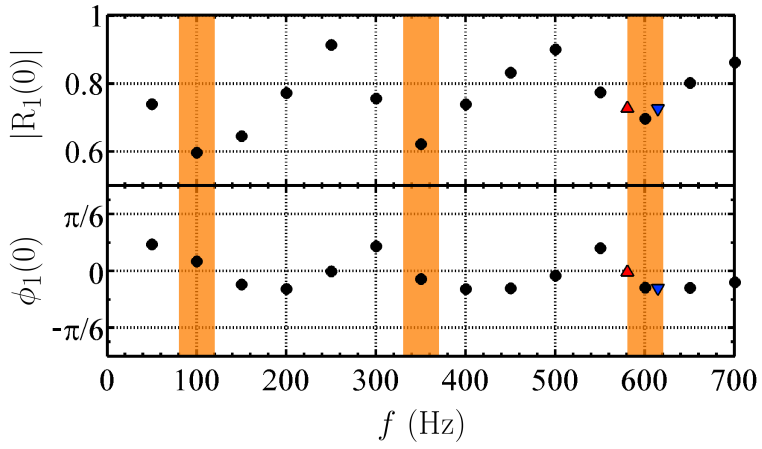

Figure 11: Reflection coefficient of the piston head $R_1(0)$. The colored regions correspond to frequency bands where the modulus features a singularity and influences the acoustic wave interacting with the piston. The downward-pointing (blue) and upward-pointing (red) triangle symbols indicate the frequencies measured in Fig. 9.

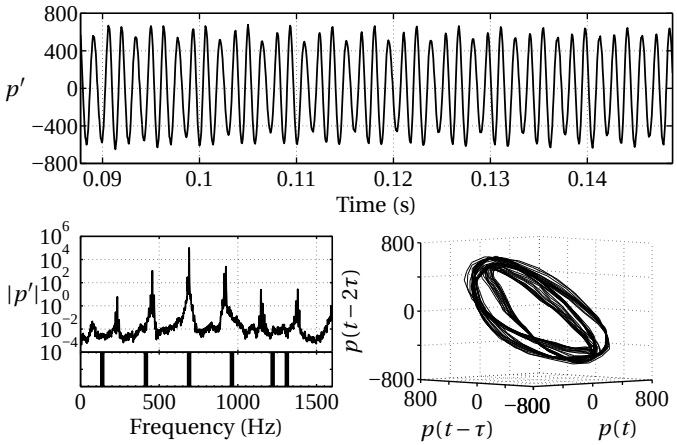

Figure 12: Pressure signal recorded by microphone M_2 (top) for $L_2 = 0.10$ m and $L_1 = 0.58$ m. The spectrum (left) and phase space reconstruction (right) are displayed in the bottom row. Acoustic eigenmodes calculated without unsteady flame but by assuming different temperatures in each cavity are plotted as vertical lines below the pressure spectrum ($T_1 = 300$ K and $T_2 = 900$ K).

typified by the existence of a linearly and a nonlinearly unstable modes, the linearly unstable mode vanishes as the instability amplitude increases and the system switches to a well defined limit cycle at a higher amplitude at the frequency of the nonlinearly unstable mode [6, 8]. There are other cases where the first mode does not vanish and both modes may be observed in the time traces [27]. A simple criterion based on the FDF calculations is suggested here to sort out situations with single or multiple frequency oscillation states [13].

The instabilities investigated correspond to the gray square symbols presented in Fig. 7 between $L_1 = 0.51$ m and 0.55 m. Measurements were also carried out for larger cavity depths up to $L_1 = 0.77$ m, where the same kind of oscillations are observed. A typical time trace is presented in Fig. 12 together with the corresponding spectral distribution and phase space reconstruction at $L_1 = 0.58$ m. Welch's method of averaging combined with a Hanning windowing is used to estimate the power spectral densities. The phase space is reconstructed using the methods presented in [28].

The pressure oscillates at a frequency corresponding to the third mode $f_{m3} = 690$ Hz. Its amplitude is modulated with a period which is equal to three times that corresponding to the fundamental frequency $f_c = f_{m3}$. The spectrum reveals the presence of modes 2 and 3. One also finds a low frequency at 234 Hz which corresponds to the difference $\Delta f = f_{m3} - f_{m2}$. In the present case this gives rise to a period tripling phenomenon observed in the pressure record where one finds that three fundamental periods are necessary to recover the same signal value. Phase space reconstruction is obtained with the methodology described previously. One obtains an embedding dimension $d_e = 4$ while the optimal time delay τ corresponds to six periods of the sampling frequency f_s, i.e. 25.3 % of the f_{m3} frequency period. A three-dimensional space is used and the reconstruction exhibits three circular patterns corresponding to three amplitude levels induced by the period tripling characterizing this case. The phase space reconstruction allows to confirm a different behavior in comparison to the one analyzed in the previous section with $L_1 = 0.40$ m. When $L_1 = 0.58$ m, the circular patterns are not in the same plane. This reveals that the frequency changes largely with the amplitude compared to the previous case where an interaction with the acoustic boundary takes place. This analysis is especially useful for the other lengths L_1 where the spectrum is not always as clear as the one presented here. It allows to delineate different circular patterns and helps to clarify the system dynamics.

To predict the occurrence of multi-mode oscillations, it is natural to examine growth rate trajectories within the FDF methodology. First, it is found that dual mode oscillations appear when there is a modal overlap, i.e. when the regions of positive growth rates of two modes intersect. A detailed examination reveals two types of overlap. The first type corresponds to two linearly unstable modes which character-

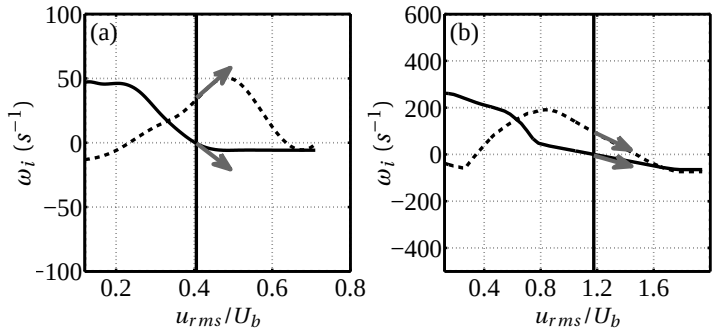

Figure 13: Growth rate trajectories calculated with the FDF. The dashed line (- -) shows the second mode growth rate, while the bold line (–) corresponds to the third mode. (a) pertains to calculations from [8] for L_1 = 0.54 m and L_2 = 0.10 m. In this case, the trajectory cross leading to mode switching during the growth of oscillation. (b) is obtained from the present investigation for L_1 = 0.52 m and L_2 = 0.10 m. Experiments reveal oscillations sustained by two modes. The first trajectory crossing $\omega_i = 0$ is indicated by means of a vertical line. Gray arrows at this point represent the tangent lines and provide the signs of the slopes for the two modes.

izes the range between L_1 = 0.43 m and 0.48 m (see Fig. 7). In this case, the second mode dominates over the whole amplitude range. This problem was examined theoretically by [25] where it is found that the dominant mode is not always reached at limit cycle. Nervertheless, by reading the bifurcation diagram, one expects that the oscillation will be locked on the mode which has the highest growth rate. This is well observed experimentally and in the corresponding range the second mode of oscillation prevails with an amplitude which closely matches that determined from the FDF calculation. It is well verified in this case that the third mode does not arise in the power spectrum. This kind of modal overlap has already been considered in previous calculations and experiments [7] which all confirm that the mode with the highest growth rate values is dominant.

The second type of modal overlap is found in the present experiments when L_1 >0.48 m, in the range where the second mode becomes nonlinearly unstable while the third mode is linearly unstable. In these cases, the two modes are sustained. The existence of linearly and nonlinearly unstable modes is a necessary condition for a dual mode of oscillation but this is not sufficient. Indeed, previous experiments indicate that when this condition is verified the two modes do not always persist simultaneously. In the unconfined geometry discussed in [6] and in the confined configuration explored in [8] it was found that the oscillation begins at the third mode frequency and that as the amplitude increases mode switching takes place and the second mode prevails. The final outcome is a limit cycle corresponding to a vanishing growth rate of the nonlinearly unstable mode ($\omega_i = 0\ s^{-1}$). It is then necessary to find the additional condition which distinguishes situations where a single mode takes over from that where the two modes are sustained. This is accomplished by examining the growth rate trajectories obtained by plotting this quantity with respect to the amplitude of oscillation.

An example is given in Fig. 13. Two configurations are shown where the trajectory of a linearly unstable mode (LUM) crosses that of a nonlinearly unstable mode (NLUM). The first case examined in Fig. 13(a) corresponds to experiments reported previously [8] in which mode switching was observed and predicted for different operating conditions. The second case, shown in Fig. 13(b), pertains to the present investigation for L_1 = 0.52 m. The amplitude level where the linearly unstable mode (LUM) trajectory crosses the horizontal axis $\omega_i = 0$ is plotted as a vertical bold line in these two diagrams. Two arrows denote the tangent lines to the growth rate trajectories at this particular amplitude level designated as a_0. In the case shown in Fig. 13(a) which gives rise to mode switching, the slope of the third mode (LUM) growth rate is negative while the slope of the second mode (NLUM) growth rate is positive :

$$(d\omega_{i3}/da)_{a_0} < 0 \text{ and } (d\omega_{i2}/da)_{a_0} > 0 \tag{1}$$

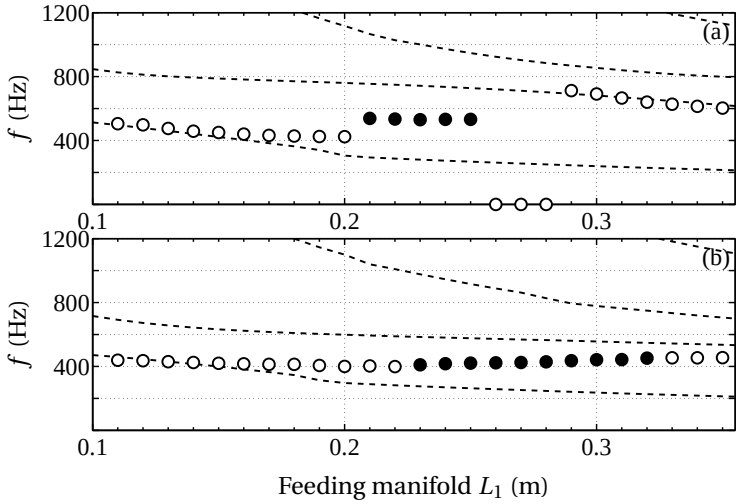

Figure 14: Instability frequency evolution as a function of the feeding manifold length L_1. (a) and (b) are respectively linked to experiments carried out with L_2 = 0.20 m and 0.30 m flame tubes. Dashed lines correspond to the acoustic eigenmodes calculated in the absence of combustion. (∘) symbols represent the peak frequency of the pressure spectrum measured by microphone M_2 for stable limit cycles. (•) symbols indicate the main frequency appearing in the spectrum of GLCs.

In contrast, when the two modes are simultaneously sustained, the growth rate slopes are both negative as illustrated in Fig. 13(b) :

$$(d\omega_{i3}/da)_{a_0} < 0 \text{ and } (d\omega_{i2}/da)_{a_0} < 0 \tag{2}$$

The present experiments indicate that when there is a modal overlap involving a linearly unstable mode (LUM) and a nonlinearly unstable mode (NLUM) and when condition eqn (2) is satisfied the oscillation takes place at the two frequencies. On the other hand, when condition eqn (1) is satisfied, mode switching takes place and the nonlinearly unstable mode prevails.

By applying the previous criterion it is possible to delineate the region of feeding manifold lengths L_1 where one expects oscillations at two modal frequencies [13]. Conditions on the two types of trajectories and the slopes of growth rates are satisfied for $0.50 \leq L_1 \leq 0.61$ m and one expects to find a double mode oscillation. The boundaries of this range nearly match those found in the experiment which is located between 0.52 m and 0.64 m. The small differences may be attributed to difficulties in determining the FDF precisely for large fluctuation amplitudes.

In summary, it is more difficult to capture the correct oscillation frequency and amplitude through the FDF framework in regions of double mode oscillations (see Fig. 7). Nevertheless, this framework allows to determine whether mode switching or double mode oscillations prevail. It appears that double mode oscillations can be expected when a linearly and a nonlinearly unstable modes overlap and when in addition condition (2) on the rates of change of the growth rates is satisfied.

5.3 Galloping limit cycles

A third class of limit cycle is observed with long flame tubes L_2 = 0.20 m, 0.30 m and 0.40 m. In this group, the amplitude is more perturbed than the ones examined previously. The system features oscillations characterized by multiple frequencies, amplitude modulation and irregular bursts which can be designated by “galloping” limit cycles or GLC. These limit cycles have been studied in [14] and the main results are presented in what follows.

Self-sustained combustion oscillation regimes are examined once more when the feeding manifold length is varied. Results are presented in Fig. 14 for L_2 = 0.20 m and 0.30 m. Combustion is initiated for

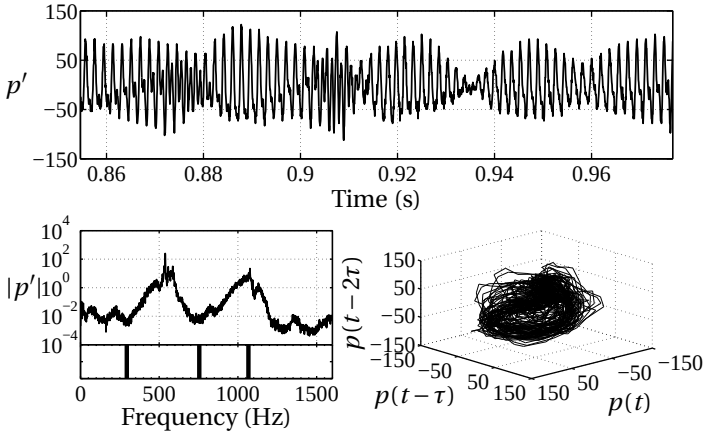

Figure 15: Pressure signal recoded by microphone M_2 (top) for $L_2 = 0.20$ m and $L_1 = 0.21$ m. The corresponding spectrum is displayed below on the left and the phase plane is shown on the right. The acoustic eigenmodes calculated without unsteady flame, but with 300 K in the feeding manifold and 1100 K in the flame tube are drawn below the pressure spectrum.

$L_1 = 0.11$ m and the feeding manifold length L_1 is increased by steps of 1 cm until $L_1 = 0.55$ m.

Stable limit cycles are indicated in Fig. 14 as open circle symbols (∘). One can see that the frequency lies close to the first acoustic mode of the combustor when L_1 is located between 0.11 m and 0.14 m. This appears for both flame tubes $L_2 = 0.20$ and 0.30 m. For sizes greater than $L_1 = 0.14$ m, the oscillation frequency is shifted with respect to the acoustic eigenmode. It is interesting to note that this frequency shift may reach 100 Hz. It clearly shows that linear stability analyses only yield a rough estimate of the frequencies which may develop in the system. One can see in Fig. 14(a) that the oscillation frequency is shifted, but the limit cycle remains stable until $L_1 = 0.20$ m for the $L_2 = 0.20$ m flame tube. In Fig. 14(b), $L_1 = 0.22$ m represents the last stable limit cycle when $L_2 = 0.30$ m. By doing the experiments, the auditive signature and the time trace indicate less organized motions of the oscillation. Thus one would qualify these oscillations as chaotic. Nevertheless, it is important to take a deeper look at the signals to confirm this point.

Phase space reconstruction and spectral analysis give insight on the periodicity and chaotic behavior of the system dynamics. As explained in [29] the "grassy appearance" of a pressure spectrum and the non periodic character of the autocorrelation function reveal the chaotic nature of the oscillation. The phase space reconstruction enables to follow trajectories and reveals possible periodic patterns or a less organized chaotic motion. It might be worth using system dynamics theoretical tools to define the attractor type and the route to chaos by calculating Lyapunov exponents or fractal dimension [15] but this will not be pursued here because the aim is to interpret the dynamical behavior of GLCs in terms of FDF calculations.

Figure 15 presents the time trace recorded for $L_1 = 0.21$ m and $L_2 = 0.20$ m. This unstable operating condition observed at the beginning of the GLCs band is characterized by a pressure oscillation between 0 and 100 Pa. The instability starts and stops randomly. By analyzing the pressure spectrum, one observes a wide peak base stretching over approximately 200 Hz. To characterize this limit cycle one uses the time series analysis presented in the previous section. The false nearest neighbors method reveals an embedding dimension of $d_e = 4$. The optimal time delay τ takes six periods of the sampling frequency $\tau \simeq 6/f_s$. In such a case it is standard to examine a three-dimensional phase space. It should be noted that the embedding dimension, determined for the other GLCs appearing between $L_1 = 0.22$ m and 0.25 m, is also $d_e = 4$. One can see in Fig. 15 that the phase space reconstruction fills a region of the embedding space without any regular structure. The oscillation travels randomly in a three-dimensional volume indicating that its behavior is chaotic in nature. The same type of result was found for the whole range of lengths L_1 where GLCs prevail.

It is now interesting to examine these results within the FDF framework to understand the observed

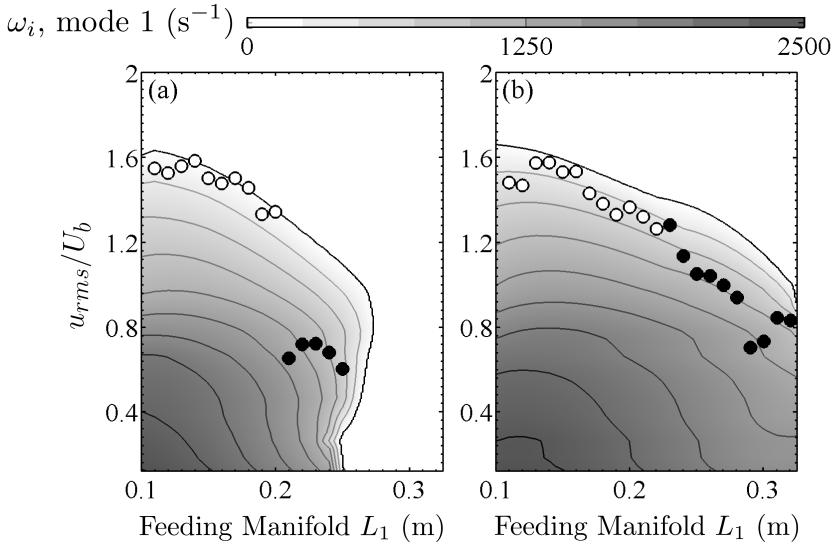

Figure 16: Growth rate evolution for the two flame tubes (a) $L_2 = 0.20$ m and (b) $L_2 = 0.30$ m. Experiments are depicted by means of symbols. Open circle symbols (∘) indicate stable limit cycles. Filled circle symbols (•) represent the peak amplitude of galloping limit cycles.

limit cycles and attempt predictions. Results are presented for the first acoustic eigenmode corresponding to the oscillations characterized experimentally. Calculations indicate that in this range of manifold length L_1, positive growth rates exist only for the first mode and this is true for both flame tube lengths L_2. Results for the growth rate ω_i are first examined in Fig. 16. This figure shows positive growth rate values in the range of lengths L_1 investigated for the two flame tubes $L_2 = 0.20$ m and 0.30 m explored. It is assumed here that the limit cycle is reached when the growth rate vanishes $\omega_i = 0$. Figure 16(a) represents calculations for the $L_2 = 0.20$ m flame tube and Fig. 16(b) shows results for the second flame tube $L_2 = 0.30$ m. Measurements are depicted with the convention used in Fig. 14. Open circle symbols (∘) indicate the oscillation amplitude of stable limit cycles. For the GLCs, the main frequency of the pressure spectrum is considered. By passing the modulated signal in a Butterworth bandpass filter one extracts the amplitude which is represented by dark circle symbols (•).

The limit cycles with stable amplitude are well predicted by calculation, but the amplitude for the GLCs is overestimated. This result is expected as the system is typified by oscillations of unstable amplitudes which may not reach the predicted level. The dark circle symbols indicate that the amplitude is mainly located around the low values. It is also possible to compare the predicted frequencies. The results are not presented here for conciseness, but they are in very good agreement with the experiments. Differences arise only in the GLC range as the amplitude calculated for $\omega_i = 0$ is not attained in the experiments.

It is now interesting to analyze results found with the FDF model to assess the origins of the GLCs. The continuation methodology employed to solve the nonlinear dispersion relation is used to track the roots of this equation as a function of amplitude u_{rms}/U_b and for each length of feeding manifold L_1. This reveals some distinct features of the roots giving rise to GLC type oscillations around the first mode. For unstable operating conditions characterized by positive growth rates $\omega_i > 0$, the solution of the dispersion relation normally features one or sometimes two modes with positive growth rates for each feeding manifold length L_1 and small disturbance amplitude levels u_{rms}/U_b. By solving the dispersion relation for increasing amplitudes, the solutions generally feature an imaginary component ω_i dropping to zero and defining the limit cycle. There are however cases where multiple solutions arise with nearly equal angular frequencies ω_r. It is then more difficult to track the roots in the complex plane as a function of amplitude. Multiple solutions may feature positive and negative ranges of growth rates ω_i. These multiple solutions are now examined and it is shown that they are present when one observes

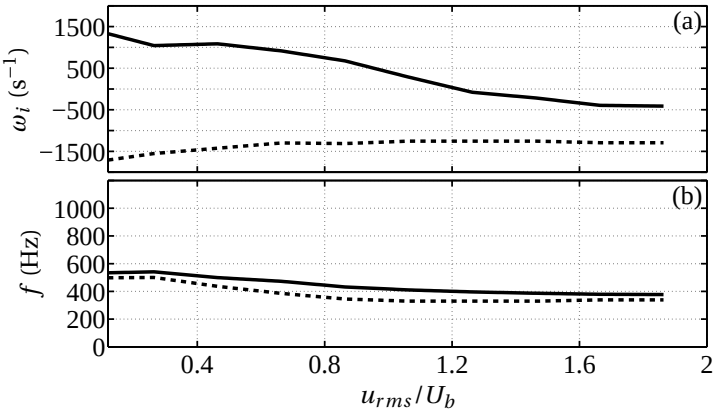

Figure 17: Growth rate and frequency evolutions for the two solutions of the first mode calculated at L_1 = 0.23 m and L_2 = 0.20 m. (a) represents the growth rates ω_i. (b) corresponds to the frequencies. Dashed lines are linked to the negative growth rate solution while the bold line corresponds to the positive one.

a chaotic limit cycle.

The evolution of the instability frequency and growth rate are here examined as a function of amplitude. Multiple solutions with positive and negative growth rates can be ignored when their oscillation frequencies differ. When the oscillation frequency ω_r of two solutions coincide or nearly coincide, one has to consider that the oscillation can grow ($\omega_i > 0$) or decay ($\omega_i < 0$). Calculations reveal two different evolution types. The first is characterized by roots featuring a negative and a positive growth rate evolving at nearly the same frequency for all perturbation amplitudes. In the second type, the roots feature a positive and a negative growth rate with coinciding frequencies in a finite range of amplitudes. The first type of solutions is depicted in Fig. 17.

The overlap of the oscillation frequency in the amplitude interval for the two solutions corresponding to mode one is presented in Fig. 17 for a case where L_2 = 0.20 m and L_1 = 0.23 m. Analysis of the growth rates plotted in Fig. 17(a) shows that even if the negative contribution is of the same order as the positive one at low amplitude, it becomes more important when the perturbation level increases. This indicates a higher damping rate than a growth rate along the trajectory for $u_{rms}/U_b > 1$. The frequency evolution plotted in Fig. 17(b) shows that the overlap is quasi-perfect for oscillation amplitudes lower than $u_{rms}/U_b = 0.35$. The largest difference between the two frequency trajectories reaches 87 Hz. This type of multiple solutions with frequency match occurs for operating conditions between L_1 = 0.22 m to 0.27 m which includes the stable band. In addition, it is also instructive to note that the dual solution band includes the chaotic limit cycles spanning between L_1 = 0.21 m and 0.25 m. Considering the overlap in oscillation frequency for the whole amplitude range, one expects that velocity disturbances will grow from $u_{rms}/U_b = 0$ to the limit cycle. However perturbations do not reach a constant amplitude limit cycle, because there is another modal solution at the same frequency characterized by a negative growth rate. A possible scenario is that of an energy transfer taking place between these modes, the growth rate becoming negative and the amplitude of the limit cycle dropping down.

For the second flame tube L_2 = 0.30 m, the predicted dual solution frequencies only overlap over a certain range of amplitudes. One first notes that the calculated overlap of frequency trajectories with dual solutions occurs between L_1 = 0.17 m and 0.31 m, while chaotic oscillations are found between L_1 = 0.23 m and 0.32 m. The scenario is that the oscillation amplitude of the unstable mode remains bounded in a finite interval with a lower bound defined by the perturbation amplitude where the two modal frequencies match. This scenario can be further analyzed by comparing the minimum and maximum oscillation levels reached in the experiments and calculations for all the GLCs observed with the two flame tubes.

This is synthesized in Fig. 18 where growth rates are plotted for the two flame tubes as in Fig. 16. One

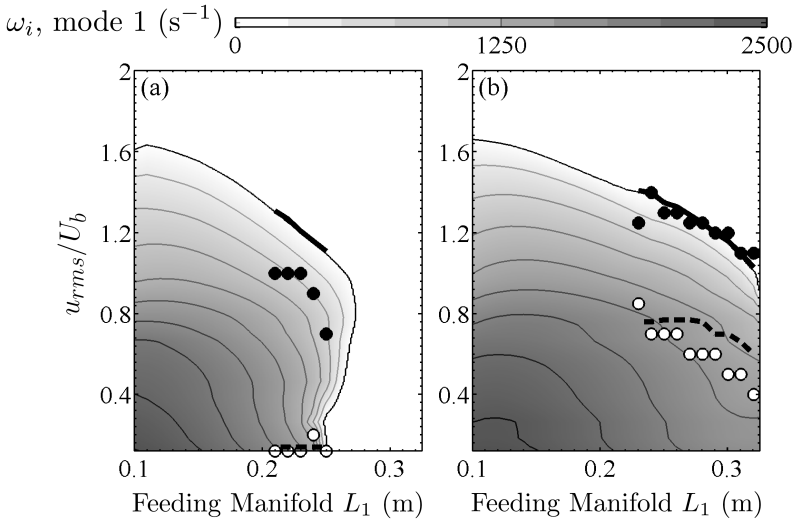

Figure 18: Growth rate evolution for the two flame tubes (a) L_2 = 0.20 m and (b) L_2 = 0.30 m. The boundary amplitudes of the experimental galloping limit cycles are represented by symbols while the boundary amplitudes where frequency trajectories overlap in calculations are shown as bold and dashed lines. Open circle symbols (∘) indicate the minimum amplitude reached in the experiments. Filled circle symbols (•) show the maximum amplitude attained. The overlap of the frequency trajectories, found in calculations, occurs for all or a part of the amplitude range. The predicted minimum amplitude is shown by a dashed line (- -) while the bold line (–) shows the limit cycle amplitude expected at $\omega_i = 0$ s^{-1}.

should note that only GLCs are considered in Fig. 18. Experiments are depicted by means of symbols. Black circle symbols (•) pertain to the maximum amplitude reached. The minimum amplitudes appear as open circle symbols (∘). These amplitudes were determined by calculating the rms values of each velocity time trace at the minimum and maximum reached during the modulation. Calculated values from the model are plotted as bold and dashed lines. The minimum amplitude where frequency trajectories overlap pertain to the dark dashed lines. The expected limit cycle where $\omega_i = 0$ is shown by the dark bold line. By examining the amplitudes reached, one can see that predictions and experimental data roughly match. For the L_2 = 0.20 m flame tube, the frequency trajectories nearly overlap for all oscillation amplitudes and one expects that u_{rms}/U_b will drop to about 0 because the negative damping rate is always higher than the positive growth rate. This phenomenon is well retrieved experimentally where the minimum oscillation amplitude vanishes. The same phenomenon highlighted for L_2 = 0.20 m is observed for L_2 = 0.30 m except that the minimum oscillation level now differs from 0. This minimum is well retrieved by considering the parameter values where the frequency trajectories, associated to negative and positive growth rates, overlap in a certain range of amplitudes.

The scenarios described previously may not give the full picture because at very high perturbation levels, which prevail in these experiments, the flame evolves significantly giving rise to rapid departures in its response. This might not be well accounted for in the FDF framework. It should be kept in mind that the FDF description assumes that the flame is perturbed around a mean state defined by the steady flow and that this may not quite reflect what is observed experimentally.

6 Conclusion

Thermoacoustic coupling was investigated in a generic combustion system featuring a feeding manifold, a multipoint injector and different flame tube lengths to confine the combustion region. A detailed model has been used by taking into account an improved description of the burner acoustic response

to flow perturbations. On the other hand, the nonlinear combustion dynamics is considered with the Flame Describing Function. First of all, results confirm that the FDF framework allows to predict self-sustained combustion oscillations in various confined configurations, a result which confirm those obtained in some recent investigations but for a simpler system (with no flame tube). The present burner configuration allows to broaden the range of investigation by disclosing new types of limit cycle. Two classes of limit cycle were identified. The first features a nearly stable oscillation amplitude, whereas the second shows amplitude and frequency unsteadiness. The first category is well described by the FDF methodology, while the second class needs a thorough examination of both experiments and calculations. It should be noted that this second category includes various oscillation states, even if the auditive signature may be the same. Examination of the time traces with different tools of signal processing such as classical spectral analysis, wavelet and nonlinear time series analysis were applied to highlight the involved phenomena. The FDF framework was also used to examine these limit cycles and try predictions or at least, understand the emergence of such states. It was possible to delineate the following aspects : (1) A first type of unsteady limit cycle characterized by regular amplitude and frequency modulations was identified. It was found that these oscillations of the limit cycle are linked to an interaction with the boundary condition. It was shown that these states are embedded in a region where the inlet reflection coefficient features a singularity. By examining FDF calculations, it was possible to propose a scenario to interpret such cases. (2) Another type of unsteadiness with periodic modulations was found when two modes are simultaneously unstable. The limit cycle is regularly distorted due to frequency heterodyning. This originates from the combination of the two modes input to the nonlinear oscillator formed by the flame. It was shown that such a process can be anticipated by examining growth rate evolution of the two modes with FDF calculations. A double mode oscillation is shown to occur when two conditions are fulfilled. (3) The last type of unsteady limit cycles is typified by irregular variations of the oscillation amplitude corresponding to irregular occurrence of starts and stops in the oscillation. These “galloping” or chaotic limit cycles (GLCs) occur in the present experiments when the system resonates in the vicinity of its first mode for small sizes of the feeding manifold cavity L_1. On the modeling level, the interpretation of the GLCs is less easy but it was found that their range of occurrence corresponds to parameter values for which the nonlinear dispersion relation of the system features roots which are closely matched in angular frequencies but have positive and negative growth rates. By determining the parameter values for which such unstable and stable modes simultaneously exist with nearly similar eigenfrequencies, it was possible to define ranges where one expects to find GLCs. This was used to explain the galloping features observed. It was shown that the calculated ranges of geometry L_1 nearly correspond to those identified experimentally. It was also shown that the FDF can be used to obtain some estimates of the maximum and minimum levels in the signal envelope. In general, the FDF framework can be used to analyze constant and time-varying amplitude limit cycles. For constant amplitude limit cycles, FDF calculation provides quantitative estimate of the oscillation frequency and amplitude. For the unstable oscillation levels, limit cycle is never attained, but the right unstable mode is predicted and the amplitudes and frequencies, found with the growth rate and frequency trajectories, lie close to the observations. Even though amplitude and frequency variations as a function of time are not reproduced, the FDF framework helps to interpret the results, enables to derive selection criteria or provides bounds of the oscillation amplitude. This framework uniquely provides informations on the many nonlinear dynamical phenomena observed in a generic combustion system at a relatively low experimental and computational effort, provided that the FDF is well measured and that the combustor acoustic response is well reproduced by the model.

References

[1] A. Gelb and W.E. Vander Velde. *Multiple-input describing functions and nonlinear system design.* McGraw-Hill Electronic Sciences Series. McGraw-Hill, New York, 1968.

[2] A.P. Dowling. Nonlinear self-excited oscillations of a ducted flame. *J. Fluid Mech.*, 346:271–290, 1997.

[3] P.J. Langhorne. Reheat buzz: an acoustically coupled combustion instability. part 1. experiment. *J. Fluid Mech.*, 193:417–443, 1988.

[4] A.P. Dowling. A kinematic model of a ducted flame. *J. Fluid Mech.*, 394:51–72, 1999.

[5] A.A. Peracchio and W.M. Proscia. Nonlinear heat-Release/Acoustic model for thermoacoustic instability in lean premixed combustors. *J. Eng. Gas Turb. Power*, 121(3):415–421, 1999.

[6] N. Noiray, D. Durox, T. Schuller, and S. Candel. A unified framework for nonlinear combustion instability analysis based on the flame describing function. *J. Fluid Mech.*, 615:139–167, 2008.

[7] F. Boudy, D. Durox, T. Schuller, G. Jomaas, and S. Candel. Describing function analysis of limit cycles in a multiple flame combustor. *J. Eng. Gas Turb. Power*, 133(6):061502.1–061502.8, 2011.

[8] F. Boudy, D. Durox, T. Schuller, and S. Candel. Nonlinear mode triggering in a multiple flame combustor. *Proc. Combust. Inst.*, 33(1):1121–1128, 2011.

[9] P. Palies, D. Durox, T. Schuller, and S. Candel. Nonlinear combustion instability analysis based on the flame describing function applied to turbulent premixed swirling flames. *Combust. Flame*, 158(10):1980–1991, 2011.

[10] C.F. Silva, F. Nicoud, T. Schuller, D. Durox, and S. Candel. Combining a helmholtz solver with the flame describing function to assess combustion instability in a premixed swirled combustor. *Combust. Flame*, 2013.

[11] S. J. Illingworth, I. C. Waugh, and M. P. Juniper. Finding thermoacoustic limit cycles for a ducted burke-schumann flame. *Proc. Combust. Inst.*, 34(1):911–920, 2013.

[12] F. Boudy. *Analyse de la dynamique non-linéaire et du contrôle des instabilités de combustion fondée sur la "Flame Describing Function" (FDF)*. PhD thesis, Ecole Centrale Paris, Châtenay-Malabry, France, 2012.

[13] F. Boudy, D. Durox, T. Schuller, and S. Candel. Analysis of limit cycles sustained by two modes in the flame describing function framework. *C. R. Mec.*, 341(1-2):181–190, 2013.

[14] F. Boudy, D. Durox, T. Schuller, and S. Candel. Nonlinear flame describing function analysis of galloping limit cycles featuring chaotic states in premixed combustors. In *Proceedings of the ASME Turbo Expo, paper GT2012-68998*, New York, 2012. American Society of Mechanical Engineers.

[15] L. Kabiraj, R. I. Sujith, and P. Wahi. Bifurcations of self-excited ducted laminar premixed flames. *J. Eng. Gas Turb. Power*, 134(3):031502.1–031502.7, 2012.

[16] I.R. Hurle, R.B. Price, T.M. Sudgen, and A. Thomas. Sound emission from open turbulent premixed flames. *Proc. R. Soc. London*, 303(1475):409–427, 1968.

[17] B. Higgins, M.Q. McQuay, F. Lacas, J.C. Rolon, N. Darabiha, and S. Candel. Systematic measurements of OH chemiluminescence for fuel-lean, high-pressure, premixed, laminar flames. *Fuel*, 80(1):67–74, 2001.

[18] H. Levine and J. Schwinger. On the radiation of sound from an unflanged circular pipe. *Physical Review*, 73(4):383–406, 1948.

[19] S.W. Rienstra and A. Hirschberg. *An Introduction to Acoustics*. Eindhoven University of Technology, Eindhoven, 2010.

[20] T. H. Melling. The acoustic impedance of perforates at medium and high sound pressure levels. *J. Sound Vib.*, 29(1):1–65, 1973.

[21] D. Durox, T. Schuller, N. Noiray, and S. Candel. Experimental analysis of nonlinear flame transfer functions for different flame geometries. *Proc. Combust. Inst.*, 32(1):1391–1398, 2009.

[22] A.-L. Birbaud, D. Durox, S. Ducruix, and S. Candel. Dynamics of confined premixed flames submitted to upstream acoustic modulations. *Proc. Combust. Inst.*, 31(1):1257–1265, 2007.

[23] A. Cuquel, D. Durox, and T. Schuller. Scaling the flame transfer function of confined premixed conical flames. *Proc. Combust. Inst.*, 34(1):1007–1014, 2013.

[24] T. Schuller, T. Tran, N. Noiray, D. Durox, S. Ducruix, and S. Candel. The role of nonlinear acoustic boundary conditions in Combustion/Acoustic coupled instabilities. In *Proceedings of the ASME Turbo Expo, paper GT2009-59390*, pages 325–339, New York, 2009. American Society of Mechanical Engineers.

[25] J. P. Moeck and C. O. Paschereit. Nonlinear interactions of multiple linearly unstable thermoacoustic modes. *Intl J. Spray Combust. Dyn.*, 4(1):1–28, 2012.

[26] E. Awad and F. E. C. Culick. On the existence and stability of limit cycles for longitudinal acoustic modes in a combustion chamber. *Combust. Sci. Technol.*, 46(3-6):195–222, 1986.

[27] A. Lamraoui, F. Richecoeur, S. Ducruix, and T. Schuller. Experimental analysis of simultaneous non-harmonically related unstable modes in a swirled combustor. In *Proceedings of the ASME Turbo Expo, paper GT2011-46701*, pages 1289–1299, New York, 2011. American Society of Mechanical Engineers.

[28] H. D. I. Abarbanel, R. Brown, J. J. Sidorowich, and L. Sh. Tsimring. The analysis of observed chaotic data in physical systems. *Reviews of Modern Physics*, 65(4):1331–1392, 1993.

[29] B. Henry, N. Lovell, and F. Camacho. Nonlinear dynamics time series analysis. In Metin Akay, editor, *Nonlinear Biomedical Signal Processing, Dynamic Analysis and Modeling*, volume 2 of *IEEE Press Series on Biomedical Engineering*, pages 1–39. Wiley-IEEE Press, New York, 2000.